Chapter 5

RAPID STELLAR ROTATION: WIND COMPRESSED DISKS

It was forged in mills where the winter
Beats incessant; ten winters the disc
Unremitting endured the cold hammer.

William Blake, *The Book of Ahania*

In the previous Chapter we studied the effects of stellar rotation on the line-driven wind from a hot star, mainly by confining ourselves to the plane of the equator ($\theta = \pi/2$) and assuming azimuthal symmetry. In this Chapter we relax the former assumption and examine wind dynamics in the full meridional plane, while still retaining symmetry about the rotation axis. Stellar rotation influences the wind outflow through centrifugal and Coriolis forces that enforce angular momentum conservation, generally tending to deflect material toward the equatorial plane and thus enhancing the density and mass outflow there. Bjorkman & Cassinelli (1993; hereafter BC) have proposed this simple and powerful "wind compressed disk" (WCD) paradigm for explaining how rotation can deflect wind flow streamlines toward the equatorial plane to possibly form shocked disks. Owocki, Cranmer, & Blondin (1994; hereafter OCB) generally confirmed BC's kinematic picture using a numerical hydrodynamics code, but found several quantitative differences from BC's original analytic model.

Section 5.1 outlines BC's original idea of wind compression, and also discusses several subsequent refinements and insights into the general phenomenon. Section 5.2 examines in detail how oblateness and gravity darkening of the underlying star alters the radiative driving of the wind, and describes initial attempts to model how this affects the wind outflow itself. This Section incorporates results

from Cranmer & Owocki (1995) and Owocki, Gayley, & Cranmer (1996). Section 5.3 displays computed theoretical P Cygni line profiles and continuum polarization from hydrodynamical models of rapidly-rotating winds, but this modeling is still in progress. Finally, Section 5.4 presents a preliminary analysis of the dynamics of the thin shocked disk which occurs in some rapidly rotating WCD models.

5.1 The Basic Wind Compression Effect

The original model of BC contained two relatively independent components: (i) the *wind compression* that arises from the overall equatorial deflection of the wind, and (ii) the *shocked disk* which can form if compression streamlines attempt to cross the plane of the equator. OCB has shown that the approximations BC used to compute the wind compression, with several minor modifications, are essentially valid, while their model of the disk itself is less reliable. Thus, in the present analysis, we will concentrate only on extensions to the analytic wind compression, and momentarily ignore the consequences of the presence of a shocked disk.

The analytic models of BC are essentially kinematic, in that the radial wind velocity is specified as a function of radius r and colatitude θ, and centrifugal and Coriolis forces then deflect these radial streamlines toward the plane of the equator. The essential assumption of a supersonic wind (thus allowing "fluid particles" to be treated as pressureless and non-interacting Newtonian tracers) is reasonably valid, as long as the wind is assumed to be rigidly-rotating with the star below the sonic point. Thus, the particle streamlines are determined solely by the external forces: gravity and radiative acceleration. Angular momentum conservation confines these trajectories to an "orbital plane" perpendicular to the initial angular momentum vector. Although BC model the radial velocity as a "beta law" (eq. [2.119]), with v_∞ a function of the stream's initial colatitude θ_i, we can generalize to the case of arbitrary velocity laws at the pole and the equator (external to any disks). At all latitudes, we thus define

$$v_r(r/R_*, \theta_i) \;=\; v_r^{\rm pole}(r/R_p)\,[1-\Theta(\theta_i)] + v_r^{\rm eq}(r/R_{\rm eq})\,\Theta(\theta_i) \;\;, \tag{5.1}$$

where we define the "latitude interpolation" function $\Theta(\theta_i)$. This form is meant to be a generalization of BC's radial velocity fits, and indeed reduces to their model when: (1) the radial velocities are assumed to follow a beta-law, and (2) the star is spherical. This function is given by

$$\Theta(\theta_i) \;\equiv\; \frac{[1-(R_*(\theta_i)/R_{eq})\,\omega\sin\theta_i]^\gamma - 1}{(1-\omega)^\gamma - 1} \;\;. \tag{5.2}$$

The exponent γ was found, through fits to Friend & Abbott's (1986) equatorial wind models (with rotation and a uniformly bright finite disk), to be $\gamma \approx 0.35$. However,

the results of Poe (1987) indicate that for O-stars, $\gamma \approx 0.5$ (see also Ignace et al. 1996). BC and OCB specify the latitude-dependent mass flux $\dot{M}(\theta_i)$ from similar fits to Friend & Abbott's (1986) models. We have similarly generalized this formalism, given polar and equatorial values for $\dot{M}$, in order to compute the local density $\rho(r, \theta)$:

$$\dot{M}(\theta_i) \; = \; \dot{M}_{\rm pole} \left[1 - \frac{R_*(\theta_i)}{R_{eq}} \omega \sin\theta_i \right]^{\xi} \quad , \tag{5.3}$$

where $\xi \approx -0.43$ from Friend & Abbott's models, but is uniquely determined, from $\xi \; \equiv \; \log(\dot{M}_{\rm eq}/\dot{M}_{\rm pole})/\log(1-\omega)$, given the polar and equatorial values. Note, however, that strict mass conservation along streamlines demands that

$$\dot{M}(\theta_i) d(\cos\theta_i) \; = \; 4\pi \rho(r,\theta) v_r(r,\theta) r^2 d(\cos\theta) \quad , \tag{5.4}$$

and this expression is used to determine the local density $\rho(r, \theta)$. (BC; Ignace et al. 1996).

The motion in the orbital plane around an inclined azimuthal angle ϕ_i is specified by the local conservation of angular momentum, and

$$v_{\phi_i}(r, \theta_i) \; = \; \frac{\Omega R_*(\theta_i)^2 \sin\theta_i}{r} \quad . \tag{5.5}$$

Note that BC's factor of $V_{rot} \equiv V_{\rm eq} \sin\theta_i$ has been consistently replaced with $V_{rot} \equiv \Omega R_*(\theta_i) \sin\theta_i$, which is not strictly equivalent for an oblate star, but more accurately takes the whole star's rigid rotation into account. The specification of v_r and v_{ϕ_i} allows orbital trajectories to be computed, and the resulting equation of motion, found from the ratio of these two velocities, is integrated from the sonic point R_s to obtain the value of the inclined azimuthal angle traversed by the streamline,

$$\phi_i(r, \theta_i) \; = \; \int_{r'=R_s}^{r} \frac{v_{\phi_i}(r', \theta_i)}{r' v_r(r', \theta_i)} dr' \quad . \tag{5.6}$$

BC and Ignace et al. (1996) use a kinematic beta law for v_r, and are able to evaluate this integral analytically. Given these trajectories, one can determine the velocity vector field in the wind, $\mathbf{v} = v_r \hat{r} + v_\theta \hat{\theta} + v_\phi \hat{\phi}$, and the density scalar field ρ, using the geometrical relations derived by BC. Specifically,

$$v_\theta \; = \; v_{\phi_i}(\cos\theta_i \, \sin\phi) \tag{5.7}$$

$$v_\phi \; = \; v_{\phi_i}(\cos\theta_i \, \cos\theta \, \cos\phi \, + \, \sin\theta \, \sin\theta_i) \quad , \tag{5.8}$$

where $\cos\phi = \tan\theta_i / \tan\theta$, and

$$\rho \; = \; \frac{\dot{M}(\theta_i)}{4\pi r^2 v_r} \left[\cos\phi_i + \frac{\cos^2\theta_i}{\sin\theta_i} \frac{d\phi_i}{d(\sin\theta_i)} \sin\phi_i \right]^{-1} \quad . \tag{5.9}$$

Note that, in order to specify $\mathbf{v}$ and ρ for an arbitrary "grid" point (r, θ), one must first solve for the initial colatitude θ_i of the streamline which passes through the given point in the wind, and this usually involves numerically finding the root of the trajectory equation (5.6) that also satisfies BC's geometrical transformation, $\cos\theta = \cos\theta_i \cos\phi_i$.

At high latitudes, rapid rotation causes wind streamlines to deflect away from the poles and toward the equatorial plane. These fluid streamlines are diverging faster than r^2 (spherical expansion), and this affects the conservation of mass which in turn impacts on the equation of motion. Kopp & Holzer (1976) and MacGregor (1988) investigate this effect in the context of magnetically enforced non-spherical expansion, and MacGregor finds (for point-star CAK winds) that although the mass loss rate is seldom strongly affected, the asymptotic wind velocity can be enhanced in regions of rapid flow divergence. Let us derive the appropriate non-spherical expansion factor for wind over the poles of a rapidly rotating star.

Consider a small initial streamline colatitude θ_i, assuming $\sin\theta_i \approx \theta_i$ and $\cos\theta_i \approx 1 - \theta_i^2/2$. The divergence of this streamline, always infinitesimally close to the pole (thus $R_*(\theta_i) \approx R_p$), will provide the necessary non-spherical divergence factor required in the mass continuity equation. We can approximate the motion in the inclined orbital plane by

$$v_{\phi_i}(r, \theta_i) \approx \frac{\Omega R_p^2 \, \theta_i}{r} \quad , \tag{5.10}$$

and the inclined azimuthal angle ϕ_i (eq. [5.6]) is then given by

$$\phi_i(r, \theta_i) \approx \Omega R_p^2 \, \theta_i \int_{r'=R_s}^{r} \frac{dr'}{r'^2 \, v_r(r')} \quad . \tag{5.11}$$

What is needed, however, is the angle θ of the streamline itself as a function of radius. Using one of BC's geometrical transformations, and realizing that all angles are small,

$$\begin{aligned} \cos\theta &= \cos\theta_i \cos\phi_i \\ \left(1 - \theta^2/2\right) &\approx \left(1 - \theta_i^2/2\right)\left(1 - \phi_i^2/2\right) \quad . \end{aligned} \tag{5.12}$$

Neglecting fourth order terms, we find that

$$\theta(r) \approx \theta_i \sqrt{1 + (\phi_i/\theta_i)^2} \quad . \tag{5.13}$$

Note that (ϕ_i/θ_i) depends only on the radius r (eq. [5.11]), and can be computed analytically if a beta-law is assumed for the radial velocity (BC; Ignace et al. 1996).

To be able to write the mass continuity equation, we must parameterize the area of a given polar (or near-polar) flux tube. Assuming azimuthal symmetry,

$$A(r) \;=\; 2\pi \int_0^{\theta(r)} r^2 \sin\theta' \, d\theta' \;=\; 2\pi r^2 \left[1 - \cos\theta(r)\right] \quad . \tag{5.14}$$

Thus, following Kopp & Holzer (1976), this area can be written as the product of the area at the stellar surface A_* with the spherical and non-spherical factors of expansion,

$$A(r) \;=\; A_* \left(\frac{r}{R_*}\right)^2 f(r) \quad , \tag{5.15}$$

where

$$f(r) \;=\; \frac{1 - \cos\theta(r)}{1 - \cos\theta_i} \;\approx\; \frac{\theta(r)^2}{\theta_i^2} \;\approx\; 1 + \left(\frac{\phi_i}{\theta_i}\right)^2 \quad . \tag{5.16}$$

It is this non-spherical factor $f(r)$ which is inserted into the mCAK equation of motion, and which can strongly affect the wind dynamics over the pole of a rotating star (see MacGregor 1988 and Section 5.2.5, below).

5.2 The Oblate Finite Disk Factor

This Section begins the process of eliminating certain approximations used in computing the radiative acceleration on the wind. Although OCB formulated the two-dimensional (2D) wind dynamics exterior to an *oblate* stellar surface in order to properly define the centrifugally distorted hydrostatic boundary, they assumed a purely radially-directed radiation force from a spherical, non-rotating star. In order to produce more self-consistent and accurate models, we present here the theoretical formalism for including the effects of stellar oblateness, limb darkening, and gravity darkening on the radiation force. In addition, we subsequently estimate the dynamical impact of such phenomena on the winds and WCDs around B stars. The actual inclusion of such forces in the time-dependent hydrodynamics is deferred to subsequent work, however, because of their inherent complexity and the increased computational expense.

Without actually computing these complex multidimensional forces, it is difficult to assess even the sense of their effect on the resulting wind dynamics. While oblateness and gravity darkening over the equator could lead to an overall decrease in the acceleration (due to the reduced flux), the higher radiative flux emanating from the poles could in turn "pinch" the force toward the equator, thus increasing the tendency to form a disk. By computing the fully oblate and gravity-darkened vector force, we thus begin to disentangle these various competing effects from each other, as well as evaluate their relative importance in the wind and disk dynamics.

5.2.1 Geometrical Considerations

Let us set up the geometrical formalism required to compute the general radiative acceleration integrals. Consider an azimuthally-symmetric oblate star centered on an origin, with its surface denoted by spherical polar coordinates $R_*(\theta)$, θ, and ϕ, and a field point in the wind, a distance r_o from the origin, inclined an angle θ_o from the z axis, and in the x-z plane (i.e. $\phi_o = 0$). Define a new, "wind-centered" coordinate system by rotating the y axis by an angle θ_o and translating the origin to the position of the field point. Thus, the new z' axis points away from the center of the star, in the $\hat{\mathbf{r}}_o$ direction, the new x' axis points in the $\hat{\boldsymbol{\theta}}_o$ direction, and the new y' axis is parallel with the old y axis (see Figure 5.1). Using Cartesian coordinates, the transformation between the two systems is given by

$$\begin{aligned} x' &= x\cos\theta_o - z\sin\theta_o \\ y' &= y \\ z' - r_o &= x\sin\theta_o + z\cos\theta_o \ . \end{aligned} \tag{5.17}$$

To evaluate the radiative acceleration integrals, both the direct stellar intensity and the projected velocity gradient must be evaluated for arbitrary rays $\hat{\mathbf{n}}$, directed from points on the stellar surface to the field point at the transformed origin. The necessary angular integrations are thus most conveniently expressed in terms of the transformed spherical polar coordinates r', θ', and ϕ'.

Before being able to evaluate the stellar intensity $I^C(\hat{\mathbf{n}})$, it is necessary to know at what point the ray $\hat{\mathbf{n}}$ intercepts the stellar surface. For a spherical star with no limb or gravity darkening, this information is never needed, but the position-dependent effective temperature $T_{\rm eff}(\theta)$ is required in the present case to compute the stellar intensity. For a given ray $\hat{\mathbf{n}}$, specified by wind-centered angles θ' and ϕ', there are, in general, either zero, one, or two possible values of r' which intercept the stellar surface, corresponding to rays lying outside, on, or inside the limb of the star, respectively. In the case of two solutions, of course, the smaller of the two values for r' corresponds to the more physically relevant (nearer) point on the oblate surface. We find these solutions numerically by transforming the point referenced by wind-centered coordinates (r', θ', ϕ') into star-centered coordinates (r, θ, ϕ), and computing the corresponding surface radius $R_*(\theta)$. If $r = R_*$ for the given value of r', then the ray $\hat{\mathbf{n}}$ exactly intercepts the stellar surface, and the star-centered angle θ can be used to compute the gravity-darkened effective temperature, and thus the intensity.

For arbitrary locations in the wind, the direct specific intensity from points on the star is given by

$$I^C(\mathbf{r}, \hat{\mathbf{n}}) \ = \ \sigma_B T_{\rm eff}^4 \, D(\mathbf{r}, \hat{\mathbf{n}}) \ , \tag{5.18}$$

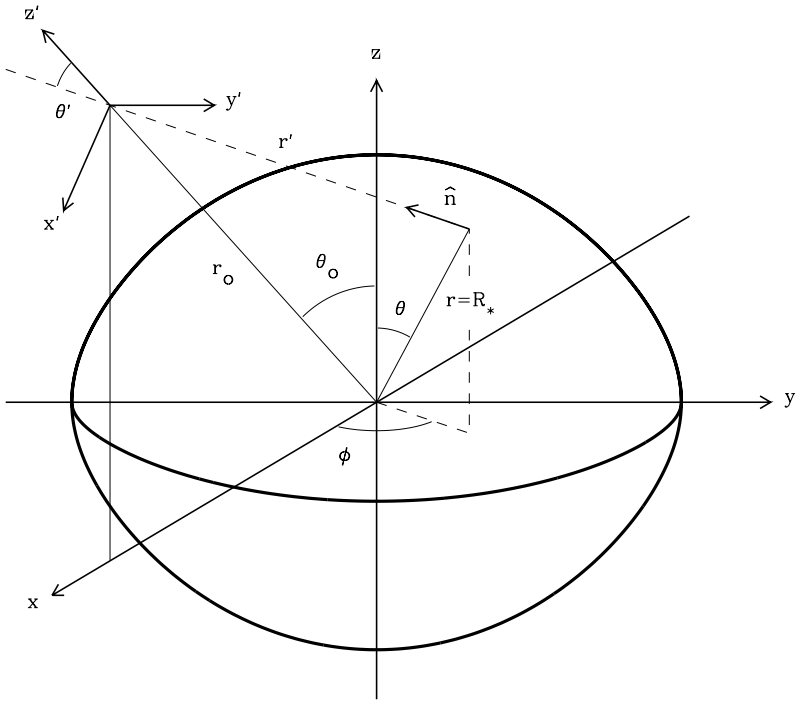

Figure 5.1: Coordinate geometry for the computation of the oblate finite disk (OFD) factor. The star-centered (un-primed) and wind-centered (primed) coordinate systems are shown, related by the position of the field point.

where the effective temperature is evaluated on the point at which the ray $\hat{\mathbf{n}}$ intercepts the oblate stellar surface. The linear limb darkening function is similar to that used for a spherical star,

$$D(\mathbf{r},\hat{\mathbf{n}}) = \begin{cases} 0, & \text{outside the limb,} \\ (2+3\mu'')/4\pi, & \text{inside the limb,} \end{cases} \tag{5.19}$$

but μ'', the cosine of the angle between the local normal to the surface (opposite the local gravity) and the ray angle $\hat{\mathbf{n}}$, must be specified more precisely by

$$\mu'' = -\frac{\mathbf{g}\cdot\hat{\mathbf{n}}}{|\mathbf{g}|} \ . \tag{5.20}$$

Note from, e.g., Figure 2 of Cranmer & Owocki (1995), that it is only for nearly equator-on views that limb darkening has a large qualitative impact on the appearance of a gravity darkened star.

The projected velocity gradient $\hat{\mathbf{n}}\cdot\nabla(\hat{\mathbf{n}}\cdot\mathbf{v})$, which resembles the rate-of-strain tensor in fluid dynamics, has been derived for a general 3D geometry by Batchelor (1967) and Koninx (1992). The assumption of azimuthal symmetry in this work somewhat simplifies this complex expression:

$$\hat{\mathbf{n}}\cdot\nabla(\hat{\mathbf{n}}\cdot\mathbf{v}) = \left(\frac{\partial v_r}{\partial r}\right)a_1^2 + \left(\frac{1}{r}\frac{\partial v_\theta}{\partial\theta}+\frac{v_r}{r}\right)a_2^2 + \left(\frac{v_r}{r}+\frac{v_\theta\cot\theta_o}{r}\right)a_3^2 + \left(\frac{\partial v_\theta}{\partial r} - \frac{v_\theta}{r}+\frac{1}{r}\frac{\partial v_r}{\partial\theta}\right)a_1a_2 + \left(\frac{\partial v_\phi}{\partial r}\right)a_1a_3 + \left(\frac{1}{r}\frac{\partial v_\phi}{\partial\theta}\right)a_2a_3 + \left(\frac{v_\phi}{r\sin\theta_o}\right)a_3a_4 \ , \tag{5.21}$$

with trigonometric factors defined by

$$\begin{aligned} a_1 &= n_r &&= n_{z'} &&= \mu' \\ a_2 &= n_\theta &&= n_{x'} &&= \sqrt{1-\mu'^2}\cos\phi' \\ a_3 &= n_\phi &&= n_{y'} &&= \sqrt{1-\mu'^2}\sin\phi' \\ a_4 &= \partial n_\phi/\partial\phi &&= -n_x &&= -\mu'\sin\theta_o - \sqrt{1-\mu'^2}\cos\phi'\cos\theta_o \end{aligned} \tag{5.22}$$

and using the standard notation $\mu' = \cos\theta'$.

Finally, we can explicitly write the oblate finite disk (OFD) factors in terms of the transformed coordinates, and following eq. (2.73),

$$\boldsymbol{\eta}^{\rm C} = \frac{4\pi r_o^2}{L_*}\oint \sigma_B T_{\rm eff}^4(\theta)\, D(\mathbf{r},\hat{\mathbf{n}})\ \hat{\mathbf{n}}\, d\mu' d\phi' \tag{5.23}$$

$$\boldsymbol{\eta}^{\rm L} = \frac{4\pi r_o^2}{L_*(\partial v_r/\partial r)^\alpha}\oint \sigma_B T_{\rm eff}^4(\theta)\, D(\mathbf{r},\hat{\mathbf{n}})\,[\hat{\mathbf{n}}\cdot\nabla(\hat{\mathbf{n}}\cdot\mathbf{v})]^\alpha\ \hat{\mathbf{n}}\, d\mu' d\phi' \ . \tag{5.24}$$

We can use the r, θ, and ϕ components of $\hat{\mathbf{n}}$ (found from the trigonometric factors a_1, a_2, and a_3 above) to obtain the respective components of $\boldsymbol{\eta}^{\rm C}$ and $\boldsymbol{\eta}^{\rm L}$. Note that η_ϕ^C is identically zero because of symmetry about the x'-z' plane in the flux. The corresponding line factor η_ϕ^L, however, is *not* zero, because the v_ϕ-component of the wind flow breaks this symmetry.

Although the OFD integrals require numerical evaluation in the most general case, the continuum OFD factor $\boldsymbol{\eta}^{\rm C}$ has a rather simple limit as the field point approaches the surface of the star (i.e. $r_o = R_*$). On the surface, the emergent vector flux is given wholly by the effect of von Zeipel gravity darkening (see Section 4.1), and depends only on the inclination colatitude θ_o,

$$\boldsymbol{\eta}^{\rm C}(r = R_*) = \frac{4\pi r^2}{L_*}\boldsymbol{\mathcal{F}} = -\frac{4\pi R_*^2(\theta_o)}{\Sigma_1}\,\mathbf{g}(\theta_o) \ . \tag{5.25}$$

Thus, using the expression for the r and θ components of the effective gravity from Section 4.1,

$$\eta_r^C(r = R_*) = \frac{4\pi GM_*}{\Sigma_1}\left[1 - \frac{8}{27}\left(\frac{R_*(\theta_o)}{R_p}\right)^3 \omega^2 \sin^2\theta_o\right] \tag{5.26}$$

$$\eta_\theta^C(r = R_*) = \frac{4\pi GM_*}{\Sigma_1}\left[-\frac{8}{27}\left(\frac{R_*(\theta_o)}{R_p}\right)^3 \omega^2 \sin\theta_o\cos\theta_o\right] \ . \tag{5.27}$$

Note that, as expected, the radial force points outward, and the equatorward (θ) force points toward the *poles*, indicating that as the star becomes more flattened, the local normal vectors to the stellar surface point more and more toward the $\pm z$ directions. The fact that $\eta_\phi^C = 0$ is evident, at least at the stellar surface, because g_ϕ is identically zero.

5.2.2 Representative B Star Model

Our basic B-star model is the standard S-350 model of OCB, a B2.5 main sequence star, chosen because it lies near the middle of the nominal range of spectral types for the Be phenomenon. Specifically, we take $M_* = 7.5M_\odot$, $R_p = 4R_\odot$, $L_* = 2310L_\odot$, and $T_{\rm eff} = 20000$ K. An equatorial rotation velocity of 350 km s^{-1} is used, because it exhibits a moderate degree of oblateness, gravity darkening, and wind compression, and it corresponds to a fractional angular velocity of $\omega = 0.89325$. We assume an isothermal wind of temperature $T_{\rm eff}$, corresponding to a sound speed of 16.53 km s^{-1}, and use the line-driving constants $\alpha = 0.51$, $k = 0.609$, and $\delta = 0.166$ (BC, OCB). In the most general case, these constants probably vary with latitude and distance from the star, but for simplicity we assume they remain fixed throughout the wind.

Table 5.1: Oblate Finite Disk Wind Models

	S-350	A	A1
$r_{\rm crit}(0°)/R_p$	—	1.06910	1.05547
$r_{\rm crit}(90°)/R_p$	—	1.35253	1.35253
$v_r(6R_p, 0°)$ (km/s)	1221.54	1098.05	1304.39
$v_r(6R_p, 90°)$ (km/s)	489.07	559.23	559.23
$\beta_{\rm eff}(2R_p, 0°)$	0.65050	0.71712	0.77445
$\beta_{\rm eff}(2R_p, 90°)$	1.41291	1.04191	1.04191
$\dot{M}(0°)$ ($10^{-10}\,M_\odot$/yr)	3.158	5.926	6.269
$\dot{M}(90°)$ ($10^{-10}\,M_\odot$/yr)	16.96	12.32	12.32
$\rho(2R_p, 90°)/\rho(2R_p, 0°)$	14.3948	8.66475	9.07238
$\max(v_\theta)$ (km/s)	74.593	60.168	58.637

Table 5.2: Oblate Finite Disk Wind Models, continued

	B	C	D	E
$r_{\rm crit}(0°)/R_p$	1.03328	1.03548	1.03614	1.03557
$r_{\rm crit}(90°)/R_p$	1.35443	1.35177	1.35153	1.35160
$v_r(6R_p, 0°)$ (km/s)	2145.33	1987.36	2001.96	2000.94
$v_r(6R_p, 90°)$ (km/s)	817.54	797.02	799.07	798.86
$\beta_{\rm eff}(2R_p, 0°)$	0.92815	0.90088	0.90325	0.90305
$\beta_{\rm eff}(2R_p, 90°)$	1.31931	1.29759	1.29928	1.29905
$\dot{M}(0°)$ ($10^{-10}\,M_\odot$/yr)	5.775	5.723	5.729	5.726
$\dot{M}(90°)$ ($10^{-10}\,M_\odot$/yr)	3.086	3.093	3.096	3.096
$\rho(2R_p, 90°)/\rho(2R_p, 0°)$	2.98853	2.84927	2.86214	2.86212
$\max(v_\theta)$ (km/s)	53.862	54.408	54.353	54.344

The wind from this model star can be specified either using the semi-analytic WCD compression paradigm or by numerically modeling the 2D wind hydrodynamics. Tables 5.1 and 5.2 show several characteristic wind quantities for the various wind models to be discussed. The standard OCB numerical model S-350, and a corresponding semi-analytic model A, are computed using the uniformly-bright spherical finite disk factor η_{un} (eq. [2.78]), evaluated using the polar value of the stellar radius at all latitudes. The polar and equatorial values of $v_r(r)$ and $\dot{M}$ for model A were computed in one dimension (1D) using a modified CAK (mCAK) code, with centrifugal forces and arbitrary finite disk factors included, and which performs the standard critical point analysis and solves the radial momentum conservation equation (see Friend & Abbott 1986; Pauldrach, Puls, & Kudritzki 1986). Abbott's (1982a) correction term for the radiative acceleration, proportional to $(\rho/W)^\delta$, is included in these models, but the standard 1D form of the dilution factor W is assumed, using the value of the stellar radius corresponding to the colatitude of the field points (i.e. either 0° or 90°). The other wind models in Tables 5.1 and 5.2 all assume the semi-analytic wind compression formalism of Section 5.1, use successive approximations to the OFD factors derived above, and will be discussed further below. The exponent $\beta_{\rm eff}$ is defined as in eq. (2.129), and the tabulated "equatorial" values from the 2D hydrodynamics code are taken at $\theta \approx 87.1°$, outside the shocked disk, in order to more clearly compare with the pure wind-compression models.

5.2.3 The Continuum Oblate Finite Disk Factor

Let us first examine the continuum OFD factor $\boldsymbol{\eta}^{\rm C}$, which depends only on the stellar intensity and not the wind. Although the continuum acceleration in O and B stellar winds is a relatively unimportant piece of the dynamical problem (because often, , $\ll 1$), we will find that, to zero order, $\boldsymbol{\eta}^{\rm C}$ and $\boldsymbol{\eta}^{\rm L}$ behave in similar ways. Thus, an understanding of the oblateness and gravity darkening effects in the former is essential for understanding the latter.

Figures 5.2 and 5.3 display the radial and latitudinal components of the continuum OFD factor, η_r^C and η_θ^C, for our representative model. Note that the dominant effect in both components follows the sense of the "sub-stellar" surface gravity darkening derived above (eq. [5.26] and [5.27]). This implies that, for an arbitrary point in the wind, most of the star's flux appears to come from an effective temperature corresponding to the point on the star nearest to the field point, where the limb darkening function is a maximum. Thus, η_r^C varies roughly monotonically, from a maximum at the bright poles to a minimum at the darker equatorial plane, and η_θ^C is negligibly small at the poles and equator, where the normal to the stellar surface is radial, and reaches a negative (poleward) maximum in the mid-latitudes.

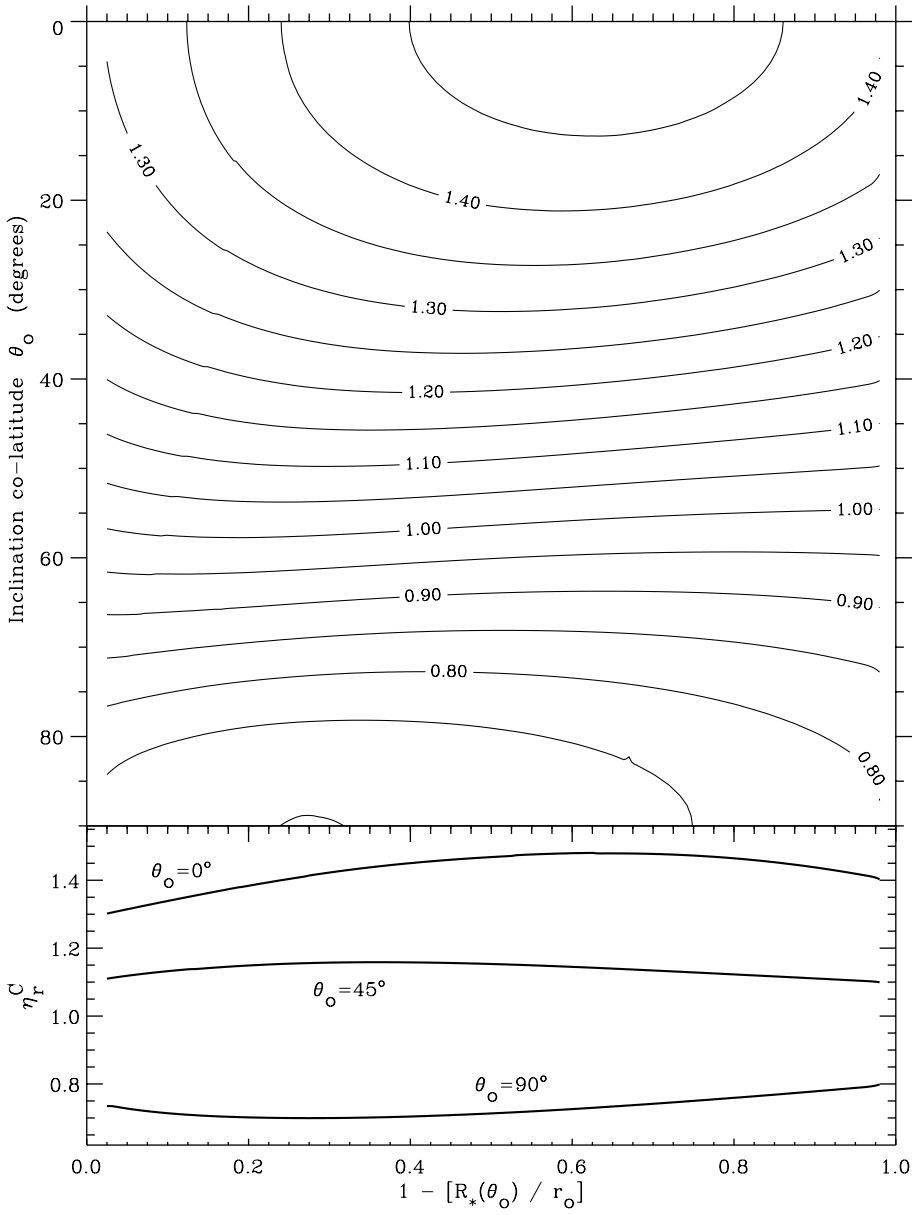

Figure 5.2: Combined contour and line plots of the **radial** (r) continuum OFD factor for the standard oblate B-star model. The line plots at the bottom of each panel illustrate the variation with radius for field points at inclinations of 0 (pole-on), 45, and 90 degrees (equator-on). The radial coordinate varies from 0 at the latitude-dependent stellar surface to 1 at infinity.

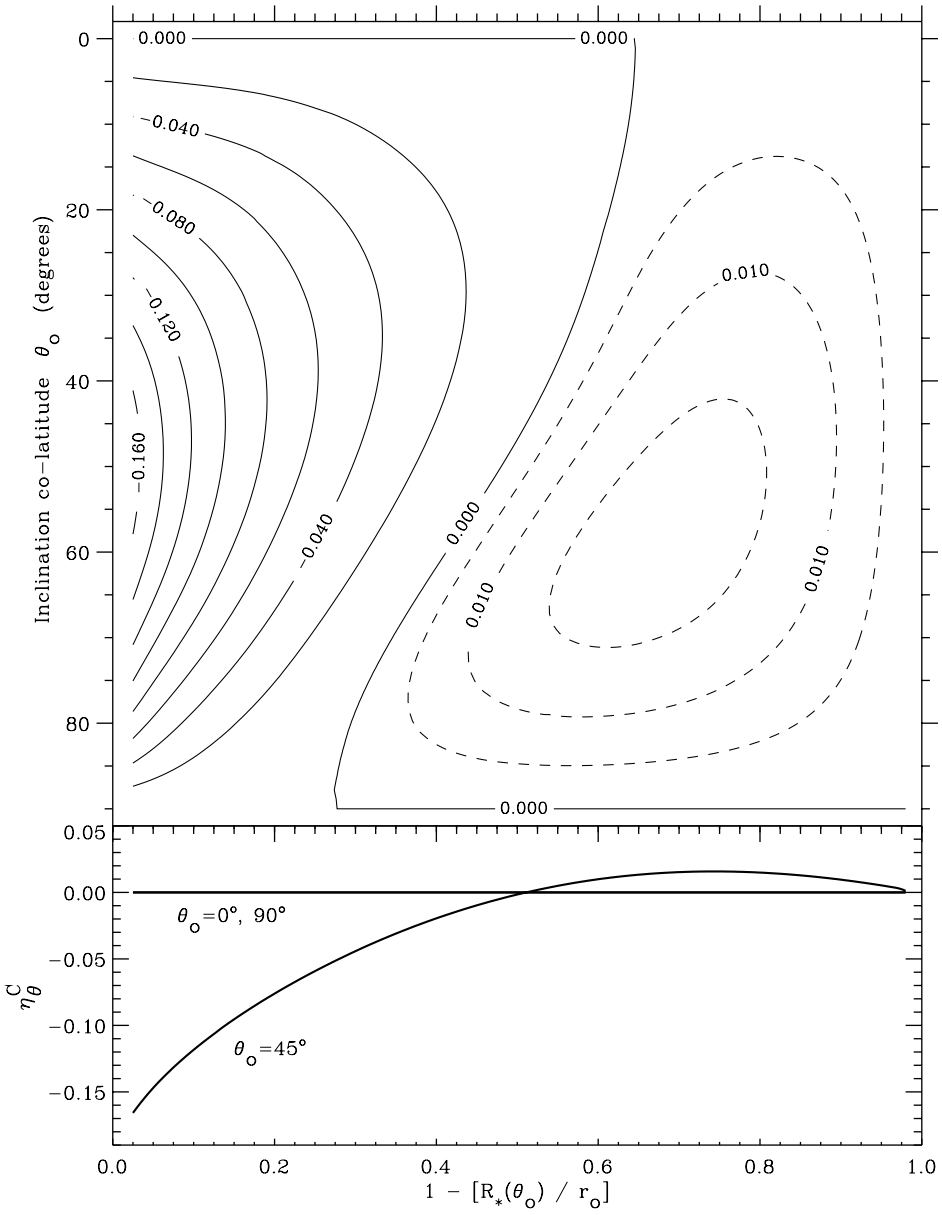

Figure 5.3: Combined contour and line plots of the **latitudinal** (θ) continuum OFD factor for the standard oblate B-star model. The line plots at the bottom of each panel illustrate the variation with radius for field points at inclinations of 0 (pole-on), 45, and 90 degrees (equator-on). The radial coordinate varies from 0 at the latitude-dependent stellar surface to 1 at infinity.

This sub-stellar gravity darkening, although dominant near the surface, is modulated by three other important effects in the circumstellar regions. First, as one moves away from the star, a larger fraction of the stellar surface, and thus a wider range of effective temperatures, is seen and integrated over. Points over the poles will see more and more of the darker equator, and points near the equatorial plane will see more of the bright poles. This effect is easily seen in η_r^C as $r_o \to \infty$, which begins to decrease near the poles and increase near the equatorial plane, and in η_θ^C, which becomes positive as $r_o \to \infty$, indicating a small degree of bright-to-dark equatorward acceleration. The second effect, which also becomes important at large distances from the star, is that the flux vector in the wind becomes more and more radial in direction, and the star appears more like a point source of flux. This primarily affects η_θ^C, driving it to zero as $r_o \to \infty$, and only weakly affecting η_r^C because the flux vector is always nearly radial.

The third effect on $\boldsymbol{\eta}^{\mathrm{C}}$ is somewhat more subtle, and has an impact at all distances from the star, but is relatively small in magnitude. The oblateness of the star causes a purely geometrical change in the continuum OFD factor, which is the ratio of the flux from an oblate surface to that from a perfect inverse-square point or spherical source. As the field point moves from the stellar surface ($r_o = R_*$) into the wind, the surface seen is either larger (over the poles) or smaller (over the equator) than is expected for a corresponding sphere extending out from the initial surface point. For example, over the pole ($\theta_o = 0$), an observer at $r_o \to \infty$ sees a circular disk with area πR_{eq}^2, but the spherical point-flux "Gaussian surface" over the poles would have radius R_p and an observed surface area πR_p^2. The ratio of the observed to the expected areas provides a rough magnitude for this effect on the OFD factors, and can be seen in η_r^C for small r_o as a slight increase near the pole and a slight decrease near the equator.

Before examining the more dynamically important line OFD factor, one final, and initially surprising feature of $\boldsymbol{\eta}^{\mathrm{C}}$ should be discussed. OCB anticipated that the inclusion of gravity darkening could lead to a "pinching" effect in the acceleration, with the force from the bright poles confining and diverting an increased acceleration toward the equatorial plane. This gravity-darkening effect is indeed seen in the limit of large r_o, but is always of negligible magnitude and dominated by the sub-stellar gravity darkening, $T_{\mathrm{eff}}(\theta_o)$. The fact that η_θ^C is negative at mid-latitudes near the star indicates that, not only is pinching toward the equator unimportant, but the flux is usually directed *away* from the equator toward the poles. Geometrically, this should come as no surprise, because the ultimate extreme of an oblate star is a flat disk, with normal vectors pointed solely in the $\pm z$ directions, away from the equator. Thus, if an enhanced equatorward force is desired for the production of stronger WCDs, it will not be found from oblateness and gravity darkening alone.

5.2.4 The Line Oblate Finite Disk Factor

The line OFD factor $\boldsymbol{\eta}^{\mathrm{L}}$ is shown in Figures 5.4, 5.5, and 5.6, and was computed using the wind velocity from the initial semi-analytic model A. The small-scale numerical noise in these figures comes mainly from the discrete computation of the velocity derivatives in the r and θ directions. To zero order, the radial factors η_r^C and η_r^L behave very similarly. Roughly, the factor η_r^L can be considered as a "convolution" of the angle integral over the oblate and gravity darkened intensity, η_r^C, and the angle integral over the projected velocity gradient term. This latter integral is given in the spherical limit by η_{un} or η_{limb}, and, to an overall accuracy of $\sim 15\%$, one can indeed model $\eta_r^L \approx \eta_r^C \eta_{un}$, where η_{un} is evaluated using the stellar polar radius. Differences between this approximation and the true value of η_r^L stem from the absence of nonradial velocity components in η_{un}, and of course from the fact that one cannot rigorously split up the integration over a product into the product of two integrals.

The latitudinal component of the line factor η_θ^L also resembles the corresponding continuum factor η_θ^C, but does not exhibit as large a range of positive values for large field point radii. Also, near the stellar surface η_θ^L approaches zero because the dominant terms in the projected velocity gradient term $\hat{\mathbf{n}} \cdot \nabla(\hat{\mathbf{n}} \cdot \mathbf{v})$ grow negligibly small for small radii. The latitudinal velocity v_θ, as well as the gradients $\partial v_\theta / \partial r$ and $\partial v_r / \partial \theta$, contribute most strongly to the latitudinal OFD factor. Near and below the sonic point, these three terms all grow small when compared to the radial gradient $\partial v_r / \partial r$ which normally dominates the finite disk factor near the stellar surface.

The line OFD factor in the azimuthal direction η_ϕ^L has no continuum counterpart, and should be understood solely in terms of the projected velocity gradient term $\hat{\mathbf{n}} \cdot \nabla(\hat{\mathbf{n}} \cdot \mathbf{v})$. Note from Figure 5.6 that this factor is always negative, and thus directed in the opposite direction from the star's rotation. The surface magnitude of η_ϕ^L implies that the wind could be significantly "spun down" from its angular momentum conserving azimuthal velocity. This fact, combined with the similarly negative sense of η_θ^L, seems to indicate that the overall effect of both nonradial OFD factors can be modeled to zero order by simply decreasing the star's equatorial rotation velocity V_{eq}. In the WCD paradigm, both v_θ and v_ϕ in the wind are most strongly influenced by the azimuthal orbital-plane velocity v_{ϕ_i}, which depends directly on V_{eq}.

The negative sense of η_ϕ^L can be understood by examining the projected velocity gradient term, equation (5.21), and noting that the only terms to produce a variation in the ϕ-component of the integrand (and thus non-cancellation when multiplied by n_ϕ) are those dependent on v_ϕ and $\partial v_\phi / \partial r$. For an outward ray $\hat{\mathbf{n}}$ tilted in the positive ϕ, or prograde direction, the projected component of v_ϕ decreases

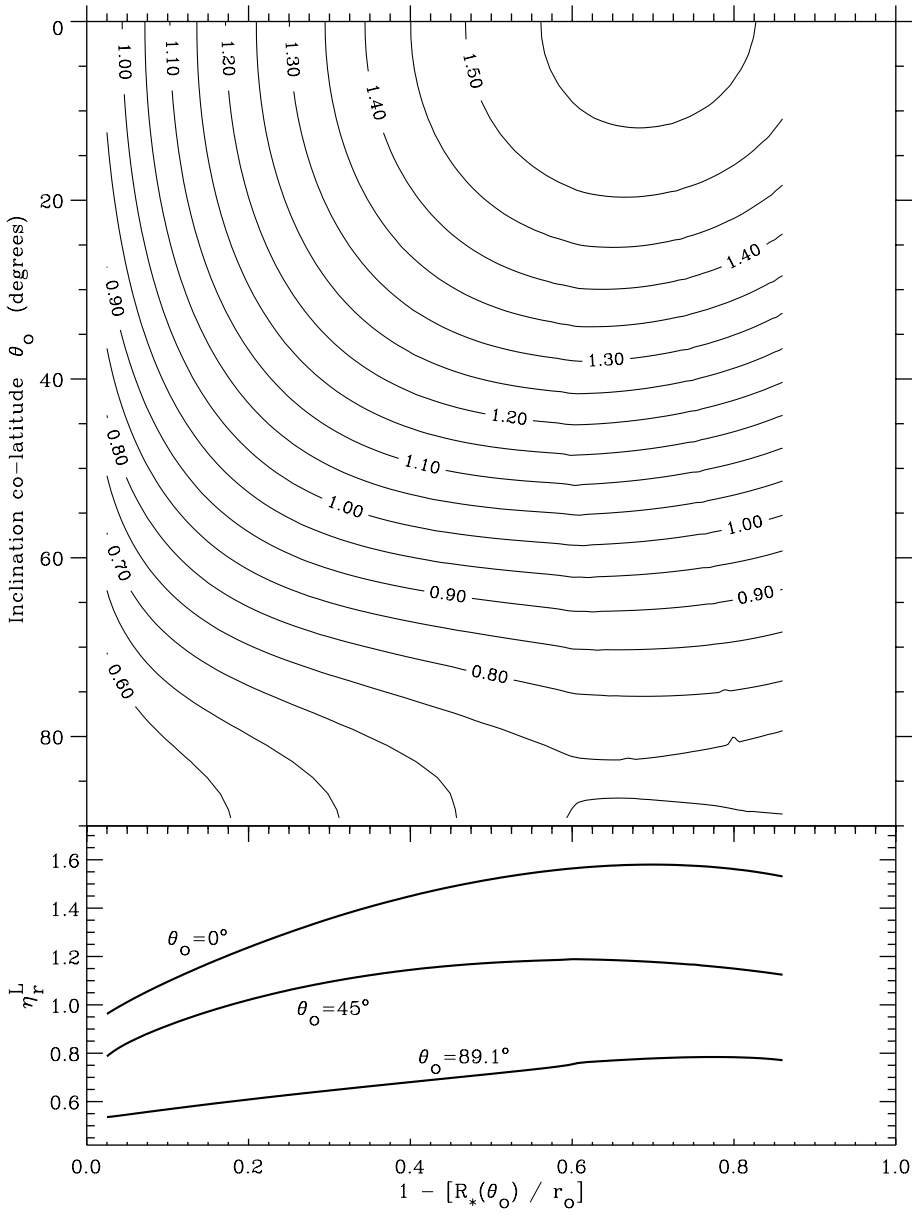

Figure 5.4: Combined contour and line plots of the **radial** (r) line OFD factor for the standard oblate B-star model, with wind specified by the semi-analytic model A. The line plots at the bottom of each panel illustrate the variation with radius for field points at inclinations of 0 (pole-on), 45, and 90 degrees (equator-on). The radial coordinate varies from 0 at the latitude-dependent stellar surface to 1 at infinity.

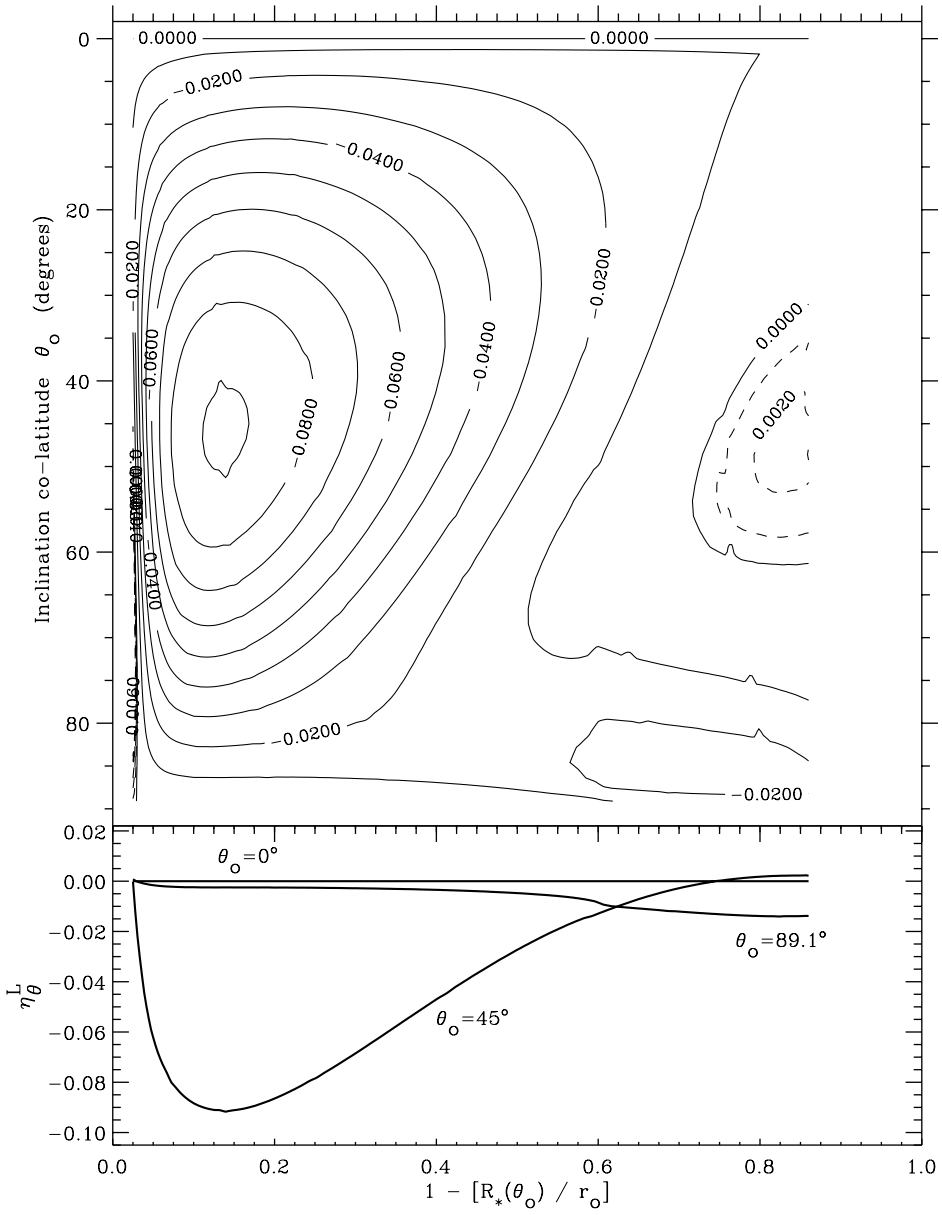

Figure 5.5: Combined contour and line plots of the **latitudinal** (θ) line OFD factor for the standard oblate B-star model, with wind specified by the semi-analytic model A. The line plots at the bottom of each panel illustrate the variation with radius for field points at inclinations of 0 (pole-on), 45, and 90 degrees (equator-on). The radial coordinate varies from 0 at the latitude-dependent stellar surface to 1 at infinity.

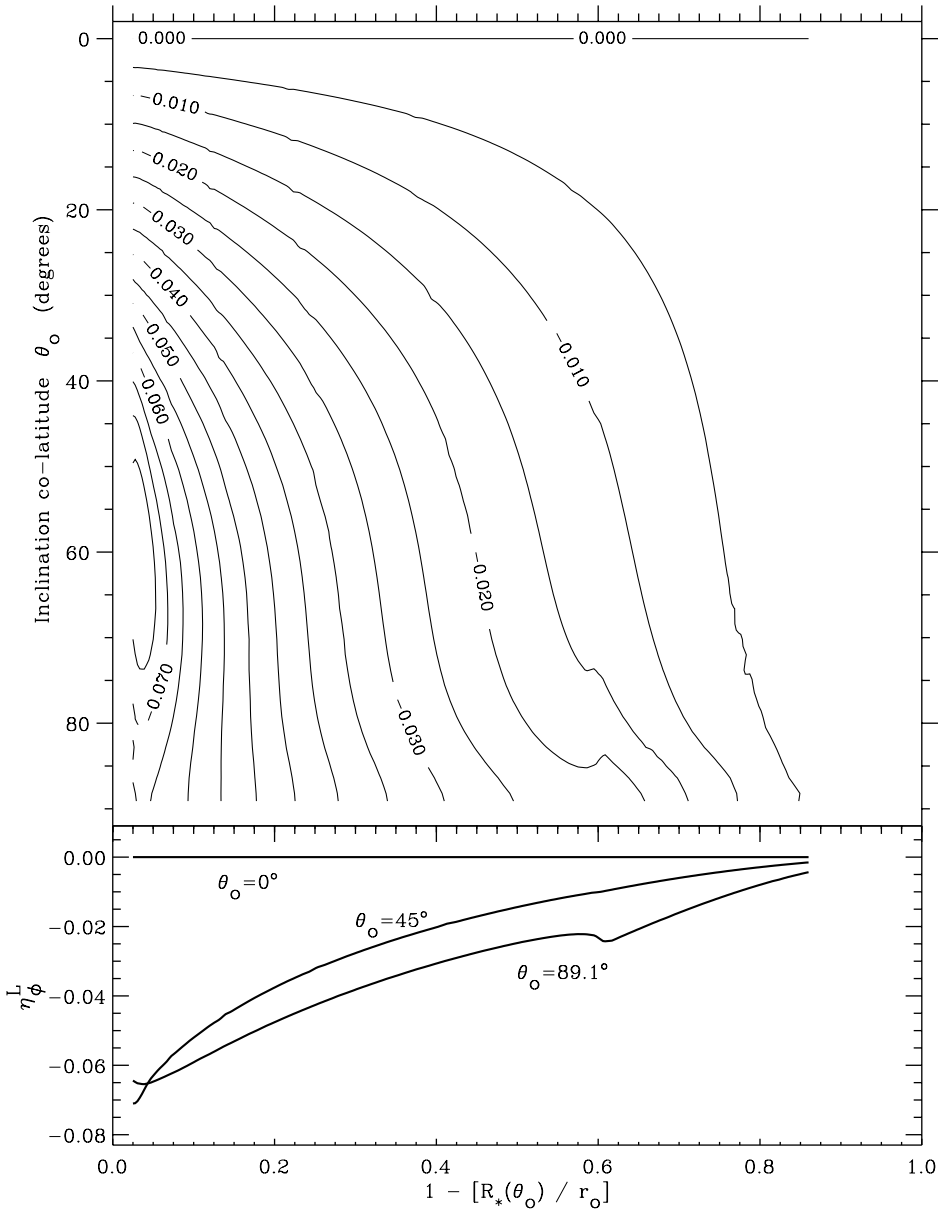

Figure 5.6: Combined contour and line plots of the **azimuthal** (ϕ) line OFD factor for the standard oblate B-star model, with wind specified by the semi-analytic model A. The line plots at the bottom of each panel illustrate the variation with radius for field points at inclinations of 0 (pole-on), 45, and 90 degrees (equator-on). The radial coordinate varies from 0 at the latitude-dependent stellar surface to 1 at infinity.

as one moves outward. However, for an outward ray $\hat{\mathbf{n}}$ tilted in the negative ϕ, or retrograde direction, the component of v_ϕ along the ray is negative, and increases (grows less negative) as one moves outward. Thus, when summed with the other, usually positive gradient terms in equation (5.21), rays in the retrograde direction have a stronger contribution to the integrand. The net effect is the "retrograde shear" (discussed in Section 4.3) that directs η_ϕ^L away from the direction of stellar rotation.

The semi-analytic model A, which provides the wind velocity field for the computation of the line OFD factor, contains only wind compression, and no shocked equatorial disk. If the velocity field of the numerical model S-350 were to be used in the computation of $\boldsymbol{\eta}^{\mathrm{L}}$, however, the presence of a disk would strongly affect the values of the line OFD factor near the plane of the equator. Although this calculation is beyond the scope of this work, its general impact should be considered. The equatorial disks found by OCB contain a drastic reduction in both the radial and latitudinal velocities, while the azimuthal velocities remain roughly continuous with the exterior wind. The gradients of v_r and v_θ, however, are maximum at the edges of the disk, where strong compression (and also high temperatures and "superionization") is thought to occur. The magnitudes of the OFD factors η_r^L and η_θ^L should be significantly enhanced in these regions, then possibly return to nearly their exterior wind values once well inside the disk. Although this enhancement provides a possible mechanism for depositing added density in the equatorial regions (through stronger latitudinal forces), definitive results will have to wait until a more self-consistent dynamical calculation is performed.

5.2.5 Effect on a Radiation Driven Wind

Once the OFD factors have been computed, we can implement them in the solution of the dynamical equations of motion and examine their overall impact on the 2D wind. However, the numerical evaluation of the OFD integrals, equations (5.23) and (5.24), is quite computationally expensive, and until recently it has been impractical to include this velocity-dependent quadrature into the time-dependent hydrodynamics. It is still possible, though, to anticipate some of the effects of oblateness and gravity darkening. First of all, because electron scattering is only a relatively minor effect in the winds of late O and early B stars (, $\ll 1$), we may ignore the impact of the continuum OFD factor $\boldsymbol{\eta}^{\mathrm{C}}$ on the dynamics of the wind. Also, in order to allow approximate 1D solutions of the equations of motion, let us consider only the impact of the radial component of the line OFD factor η_r^L on the wind over the poles and the equator. We can employ the same 1D mCAK method used for model A to find solutions for $v_r(r)$ and $\dot{M}$ along these two loci of wind points, but with the radial OFD factors used instead of the spherical finite disk

factor η_{un}. This defines the first step in an iterative process, designed to find a quasi-self-consistent wind solution:

1. Compute polar and equatorial $v_r(r)$ and $\dot{M}$ using 1D mCAK code.
2. Determine wind compression velocities in r, θ, and ϕ directions, using modified BC semi-analytic model (see Section 5.1).
3. Use this velocity field to re-integrate the OFD factor η_r^L for points over the poles and equator.
4. Repeat steps 1 to 3 until solutions settle to consistent values.

Note that, although this procedure disregards the effects of the nonradial OFD factors at all latitudes, and only estimates the radial OFD factor at mid-latitudes, it can provide a first estimate of how the overall wind compression will be affected by the presence of pole-to-equator variations in the radiative acceleration.

Before actually carrying out this iterative process, let us consider one additional, and possibly important, 2D effect: the polar streamline divergence derived above in Section 5.1. Model A1 in Table 5.1 was computed using this polar non-spherical divergence, and its polar terminal velocity (represented by the radial velocity at 6 polar radii) and its equator-to-pole density contrast agree slightly better with OCB's numerical model S-350, which naturally contains this 2D effect. In the equatorial regions there would seem to be the opposite effect – streamline convergence – but pressure forces, ignored in the simple wind compression picture of Section 5.1, act to redirect the flow into a nearly radially outflowing disk.

Starting with the original initial model A, models B through E in Table 5.2 were computed using the above iterative process and polar non-spherical divergence. Self-consistency seems to have been reached in the four iterations shown. The overall effect of the polar and equatorial radial OFD factors is a general weakening of the BC wind compression, as shown by the equator-to-pole density contrast, which is only $\sim 30\%$ of its original (non-OFD) value. Note that this density ratio does not include the shocked disk expected to form at the equator, but the strength of the disk in part depends on the amount of wind compression immediately exterior to it. The polar and equatorial wind terminal velocities are both increased by factors of 1.5 to 2, and the velocity laws using the OFD factors accelerate toward their terminal values over a longer distance (i.e., they are less "steep"). The local mass flux over the pole is virtually unchanged, while the mass flux over the equator has decreased by a factor of four. This can be understood at the pole by the competition between the generally larger OFD factor and the non-spherical divergence factor, while at the equator the generally smaller OFD factor (due to gravity darkening)

acts alone to decrease the radiation force, and thus the local amount of mass loss (see eq. [4.31]).

We caution that, although this dynamical analysis contains much of the physics derived for the OFD factors above, it ignores all nonradial force components in the OFD factor, and only treats the radial components approximately. Indeed, preliminary 2D hydrodynamical models which incorporate these OFD forces evolve to qualitatively different solutions than predicted above. Owocki, Gayley, & Cranmer (1996) show that the small *poleward* and *retrograde* forces in the θ and ϕ directions actually result in the complete inhibition of the BC equatorial wind compression effect. This conspires with the net *decrease* in $\dot{M}$ over the equator due to gravity darkening (see Section 4.2) to further decrease the predicted equatorial density enhancement. In the most rapidly rotating models there is even a density *minimum* at the equator, and bipolar higher-density "lobes" around the poles. The apparent contradiction between these (seemingly robust) theoretical results and the inferred detection of WCDs around O and B stars in several cases (e.g., Bjorkman et al. 1994; Harries & Howarth 1996) is currently being examined. Of course, as Ignace et al. (1996) have indicated, in systems where line driving and gravity darkening are not expected to occur, the BC wind compression paradigm is still likely to represent an important dynamical component of the circumstellar matter around rotating stars.

5.3 Line Profiles and Polarization

The SEI line synthesis method discussed in Chapter 3 can be extended to winds without spherical symmetry, and in this Section we present P Cygni line profiles from a representative two-dimensional axisymmetric WCD model. The oblate stellar "boundary" is taken into account numerically, and the wind's velocity and density variations in r and θ are transformed into an arbitrary observer-centered coordinate system. Figure 5.7 shows P Cygni line profiles of the A1 model wind presented in Section 5.2 above, for observers at various inclinations. The "standard" line parameters of Section 3.1.4 are used: $k_L = 1$, $\epsilon_o = 0$, $v_{\rm turb} = 100\,{\rm km\ s^{-1}}$, and $\Delta i = \gamma = 0$.

The most evident inclination-dependent variations are due to the decreasing terminal velocity and increasing mass flux from pole to equator. Note that this wind compression model does not contain a shocked disk, and thus the line profiles do not show the strong low-velocity "shelf" feature found by Bjorkman et al. (1994) in theoretical P Cygni profiles of stars with equatorial disks. More complete multi-dimensional hydrodynamical models, such as those of Owocki, Gayley, & Cranmer (1996), do not contain strong WCDs, and in fact exhibit a *decreasing* mass flux

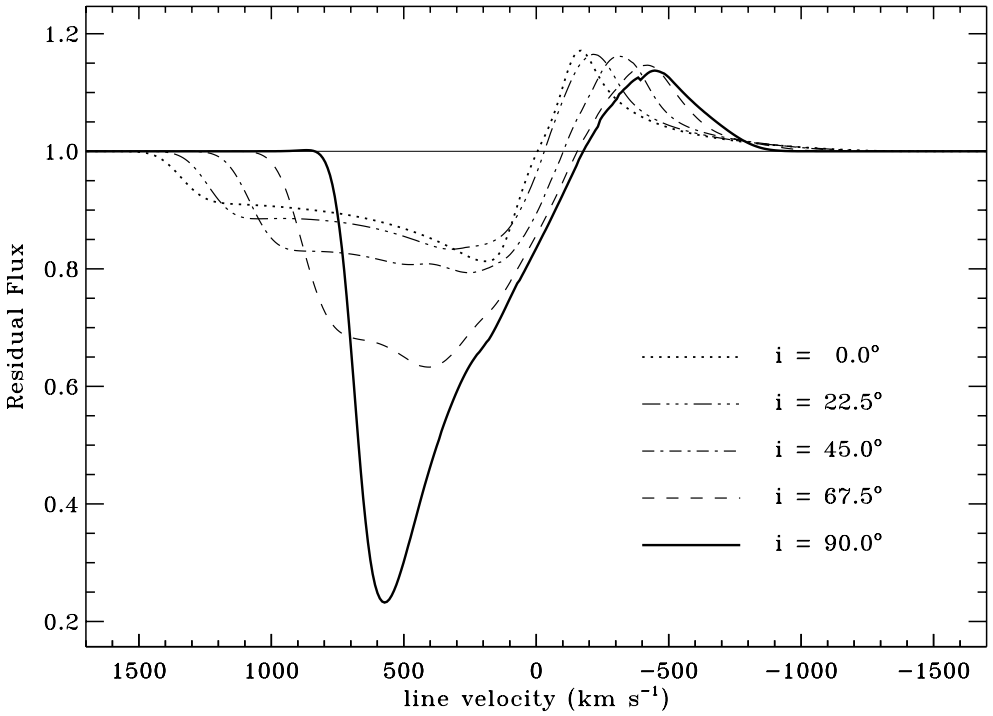

Figure 5.7: Theoretical (SEI) P Cygni line profiles for the A1 analytic wind compression model wind. Observers at $i = 0, 22.5, 45, 67.5$, and 90 degrees are shown.

from pole to equator. Preliminary computations of P Cygni line profiles and photospheric diagnostics such as Hα (see, e.g., Petrenz & Puls 1996) show significant differences between these paradigms, and this promises to aid in identifying the actual circumstellar distributions of matter around rotating O and B stars.

Figure 5.8 shows the continuum electron-scattering polarization for both the A1 wind compression model and the S-350 hydrodynamical WCD model computed by OCB. The code written to calculate this polarization integrates over the wind volume exterior to the oblate star, but performs the solid-angle integration (in, e.g., eq. [3.46]) over a non-gravity-darkened spherical surface of radius R_p. The overall approximate dependence on $\sin^2 i$, as discussed in Section 3.2 for an axisymmetric non-occulted envelope, is evident, and deviations from $\sin^2 i$ arise from the occultation of material behind the star. Note the difference in magnitude between the models with and without a shocked wind compressed disk; the polarization increases by a factor of 20 when the thin WCD is included, and its presence seems necessary to generate an observable amount of polarization in the weak winds of B stars. However, in the much denser winds of O stars, even modest wind compression without a disk can generate a significant continuum polarization ($\sim$0.3% for ζ Puppis; see Harries & Howarth 1996).

5.4 An Idealized 1D Model of the Shocked Disk

For hot stars where equatorial wind compression is present, OCB found that the dynamics *within* the shocked disk is markedly different from the predictions of Bjorkman & Cassinelli (1993). Because the Sobolev line driving scales inversely with the gas density, the material in the disk is not accelerated as strongly as the remainder of the wind, and this results in a net *inflow* of matter onto the star beneath a "stagnation point" r_o, which moves outward with increasing rotation velocity. Because of the sharp contrast between the rapid equatorial wind flow exterior to the disk and the slow pressure-confined flow interior to the disk, it may be possible to model the dynamics of the disk in one dimension, and treat the "input" of mass and momentum from the wind as an external boundary condition. Bjorkman (1992) began to construct such a model, but assumed the detached-disk paradigm of BC. In this Section we outline some of the key equations in a 1D model of a shocked disk with a stagnation point. Note, however, that this analysis is still at a preliminary stage of development, and the main purpose of this Section is to document these initial steps in the problem.

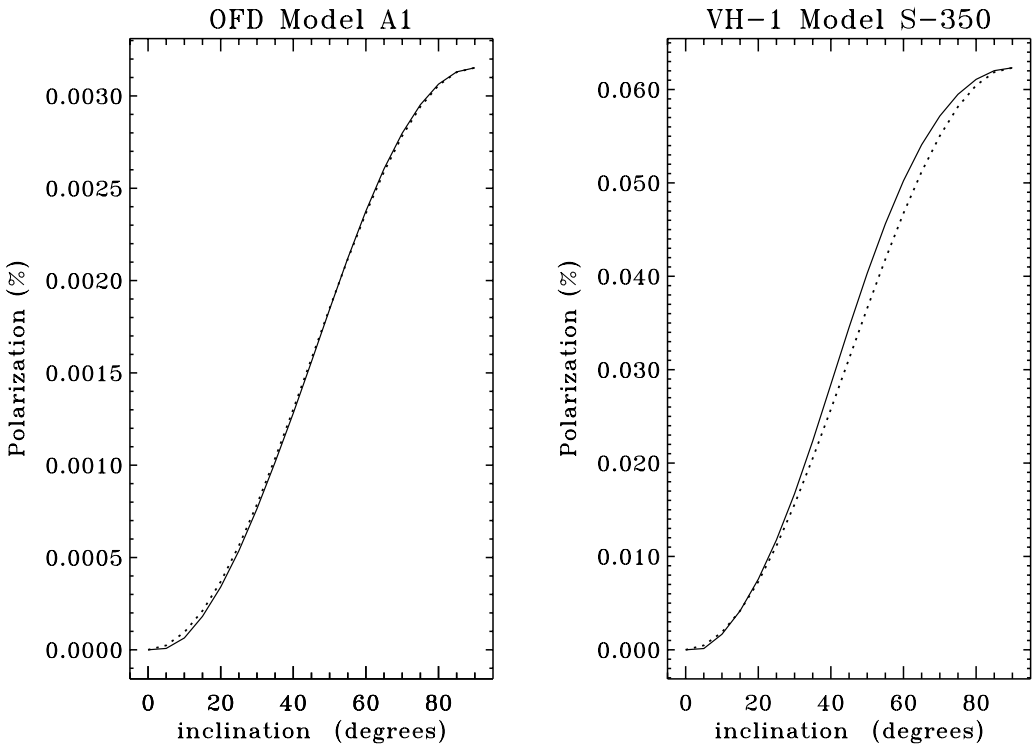

Figure 5.8: Optically-thin electron scattering polarization for the A1 analytic wind compression model (left curves), and for the S-350 numerical hydrodynamics wind model (right curves). Solid lines show the numerically-computed polarization variations with inclination, and dashed lines show the square of the sine of the inclination, normalized to the equatorial polarization.

5.4.1 Equations of Motion

In order to model the interior of a shocked equatorial wind compressed disk (WCD), several assumptions must be made. First, because numerical models have shown that the disk is extremely thin, let us consider it to be ideally *planar,* and replace the 3D volume mass density ρ with a 2D surface density σ, expressed as mass per unit area in the disk. Second, because of the relative success of the analytic wind compression model (Bjorkman & Cassinelli 1993; Owocki, Cranmer, & Blondin 1994; Cranmer & Owocki 1995), we can consider the input of mass and momentum into the disk as known, and thus write the fluid equations with "source terms" of mass and momentum deposited from the exterior wind.

In general, the 2D fluid equations of mass and momentum conservation can be written in conservative form as

$$\frac{\partial \sigma}{\partial t} + \nabla \cdot (\sigma \mathbf{v}) \; = \; j_o \tag{5.28}$$

$$\frac{\partial}{\partial t}(\sigma v_r) + \nabla \cdot (\sigma \mathbf{v} v_r) + \frac{\partial P_{\rm eff}}{\partial r} - \sigma g_r \; = \; j_r \tag{5.29}$$

$$\frac{\partial}{\partial t}(\sigma v_\phi) + \nabla \cdot (\sigma \mathbf{v} v_\phi) + \frac{1}{r}\frac{\partial P_{\rm eff}}{\partial \phi} - \sigma g_\phi \; = \; j_\phi \;\; , \tag{5.30}$$

where j_o, j_r, and j_ϕ are the source terms of mass and linear momentum in the radial (r) and azimuthal (ϕ) cylindrical-coordinate directions, respectively, and the vector $\mathbf{g}$ represents a general external acceleration. Note that the divergence operation is taken in the 2D equatorial plane only, and the effective "pressure" $P_{\rm eff}$ here has units of force per unit length.

The source terms can be written in terms of the actual mass density and flow velocity of the wind, denoted by ρ_w and $\mathbf{w}$, exterior to the disk. Consider an infinitesimally small volume δV embedded in the equatorial disk. The volume δV can be written

$$\delta V \; = \; \delta z \; \delta A \; = \; (w_z \, \delta t) \; \delta A \;\; , \tag{5.31}$$

with δA being the projected area of the volume in the equatorial plane, and δt being an infinitesimal time interval over which the wind flows through the vertical (z) extent of the volume. The vertical velocity w_z of the wind entering from above is given by $w_z = w_\theta \sin\theta - w_r \cos\theta$, but is approximately equal to w_θ itself near the equatorial plane. Although we are utilizing a continuum description of the fluid, let us momentarily define a number N of fluid particles (each of mass m) in the volume δV, and $N = \rho_w \, \delta V \, / m$. Thus, the "creation rate" of particles in the disk, per unit area per unit time, is defined as

$$\mathcal{S} \; \equiv \; \frac{N}{\delta A \; \delta t} \; = \; \frac{\rho_w}{m} \, w_z \;\; , \tag{5.32}$$

and the source terms of mass and linear momentum are given simply by

$$j_o = m\mathcal{S} \ , \quad j_r = mw_r\mathcal{S} \ , \quad j_\phi = mw_\phi\mathcal{S} \ . \tag{5.33}$$

These terms are similar to the "mass loading" sources in energetic solar-wind plasmas, where conservation of individual ionic species is violated by ionization and charge-exchange processes (see, e.g., Story 1996). Note that the wind density ρ_w and velocity $\mathbf{w}$ are functions of position, given by the Bjorkman and Cassinelli (1993) analytic wind compression model, and thus the source terms can be considered known as well.

With the derived source terms, and the assumptions of azimuthal symmetry and steady state, the fluid conservation equations in the equatorial plane become

$$\frac{1}{r}\frac{\partial}{\partial r}(r\sigma v_r) \ = \ j_o \tag{5.34}$$

$$\frac{1}{r}\frac{\partial}{\partial r}(r\sigma v_r^2) - \frac{\sigma v_\phi^2}{r} \ = \ -\frac{\partial P_{\rm eff}}{\partial r} + \sigma g_r + j_o w_r \tag{5.35}$$

$$\frac{1}{r}\frac{\partial}{\partial r}(r\sigma v_r v_\phi) + \frac{\sigma v_r v_\phi}{r} \ = \ \sigma g_\phi + j_o w_\phi \ . \tag{5.36}$$

By expressing divergences as cylindrical "slab-like" derivatives we implicitly assume a flat disk, with a constant scale height h. Later, however, we will be able to use a relationship between σ and the volume density ρ to estimate how h may vary with radius. The two above momentum equations can be simplified by appropriately separating the products in the differentiations on the left-hand side, and using the mass continuity equation. These two equations thus simplify to

$$v_r\frac{\partial v_r}{\partial r} - \frac{v_\phi^2}{r} \ = \ -\frac{1}{\sigma}\frac{\partial P_{\rm eff}}{\partial r} + g_r + \frac{j_o(w_r - v_r)}{\sigma} \tag{5.37}$$

$$v_r\frac{\partial v_\phi}{\partial r} + \frac{v_r v_\phi}{r} \ = \ g_\phi + \frac{j_o(w_\phi - v_\phi)}{\sigma} \ . \tag{5.38}$$

The quantity j_o/σ has units of inverse time, and can be considered a kind of "mass injection rate" which sets the scale for the r and ϕ accelerations.

For the present, let us leave the azimuthal momentum equation, and assume v_ϕ to be known (usually, $v_\phi \sim 1/r$, which conserves angular momentum). Note that we cannot immediately neglect the pressure gradient term in the radial momentum equation, because the wind velocity inside the disk can become arbitrarily small. If an isothermal wind is assumed, with sound speed a, and an idealized 2D equation of state $P_{\rm eff} = \sigma a^2$ is applied, the radial equation of motion can be written in terms of a mass flux variable $J \equiv \sigma v_r r$, and the two governing differential equations become

$$\frac{dJ}{dr} \ = \ j \tag{5.39}$$

$$\left(v_r - \frac{a^2}{v_r}\right)\frac{dv_r}{dr} = g_r + \frac{v_\phi^2}{r} + \frac{a^2}{r} + \frac{j_o r}{J}\left[v_r(w_r - v_r) - a^2\right] \quad , \tag{5.40}$$

defining $j \equiv j_o r = \rho_w w_z r$ as a "linear" mass flux into the disk.

The external acceleration term g_r in general contains both gravity and the effects of radiative driving:

$$g_r = -\frac{GM(1-,)}{r^2} + \frac{GM,}{r^2} k\eta\,(r, v_r, dv_r/dr)\left(\frac{1}{\sigma_e \rho v_{th}}\frac{dv_r}{dr}\right)^\alpha \left[\frac{n_e}{(10^{11}\,\mathrm{cm}^{-3})W}\right]^\delta \tag{5.41}$$

(see CAK; Abbott 1982a; Friend & Abbott 1986). In the remainder of this analysis, however, we will consider a simplified form of the radiative driving, neglecting Abbott's (1982a) ionization correction ($\delta = 0$), and assuming a point source of radiation ($\eta = 1$). Note, however, the presence of the 3D mass density ρ in the line acceleration. This can be dealt with in the present 2D model in one of two ways: (1) replace ρ by the quantity σ/h, where h is a representative radially-dependent disk scale height, or (2) use the simple ram pressure balance given by BC for an ideally flat disk,

$$\rho \approx \rho_w \left(1 + \frac{w_z^2}{a^2}\right) \quad . \tag{5.42}$$

In the following, we will use the latter assumption, and assume ρ to be a known function of radius. This implies that once we solve for $\sigma(r)$, we automatically have $h(r)$, and we can evaluate the validity of the above thin-slab approximation directly. As an aside, if we *assume* h to have a given value, this allows us to estimate σ and turn the equation of motion into a purely algebraic equation for $v(r)$. This method, though, is unreliable because of the extremely sensitive dependence on this choice for h. Finally, then, we can express the *effective* external acceleration as

$$\left(g_r + \frac{v_\phi^2}{r} + \frac{a^2}{r}\right) \equiv -g(r) + k(r)\left(\frac{dv_r}{dr}\right)^\alpha \quad , \tag{5.43}$$

with both $g(r)$ and $k(r)$ being known positive quantities.

The unknown mass flux $J(r)$ can be easily integrated, given an initial condition from which to integrate. A convenient radius to choose is the "stagnation point" r_o, at which $v_r \equiv v = 0$. Numerical studies have shown that there is an inner disk inflow ($v < 0$) below this radius, and outflow ($v > 0$) above it. Figure 5.9 shows the functions $j(r)$ and $J(r)$ for the S-350 model of OCB. Because the location of the stagnation point is not known *a priori*, $J(r)$ is known only relative to an unknown additive constant, and three representative choices are shown. Note, however, that the mass-supply function $j(r)$ is sharply peaked in radius, rapidly approaching zero both as $r \to R_*$ and as $r \to \infty$. This implies that J, its integral, varies most rapidly

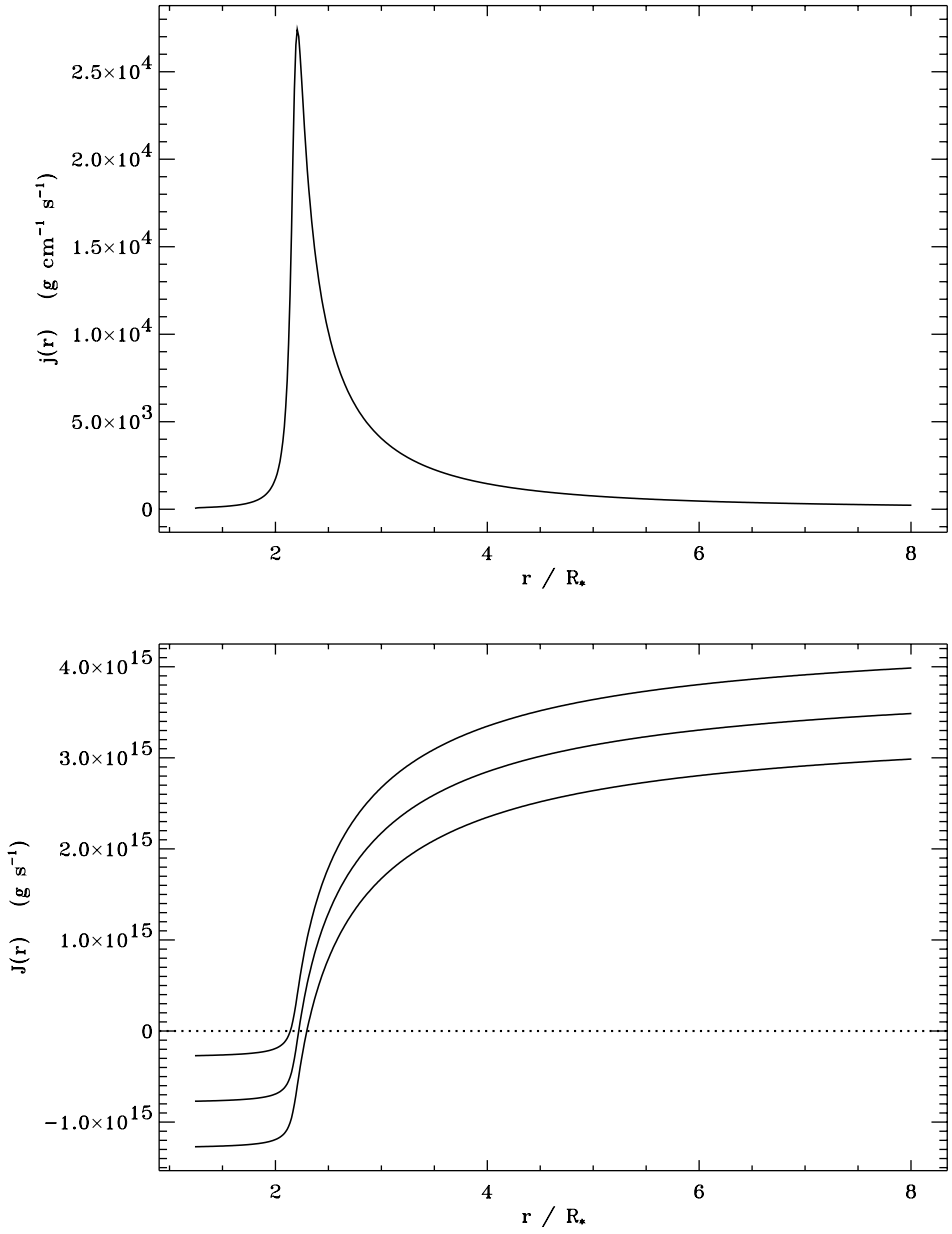

Figure 5.9: Upper curve: Mass-loading source term $j(r)$, which is sharply peaked near the stagnation point. **Lower curve:** Integrated source of mass flux $J(r)$, unknown to within an additive constant. $J(r)$ crosses zero at the stagnation point.

where j is at its peak, and should cross zero very near this point. The actual position of the stagnation point for the S-350 numerical model is $r_o = 2.03R_p$, which is close to the peak of $j(r)$ at $\sim 2.2R_p$.

We can represent the equation of motion as

$$F_1\left(r, v, \frac{dv}{dr}\right) = \left(v - \frac{a^2}{v}\right)\frac{dv}{dr} + g - k\left(\frac{dv}{dr}\right)^{\alpha} - \frac{j}{J}\left[v(w_r - v) - a^2\right] = 0 \quad . \quad (5.44)$$

If we choose $\alpha = 1/2$, it becomes possible to solve for the velocity gradient quadratically, and

$$\frac{dv}{dr} = \left[\frac{kv}{2(v^2 - a^2)} \pm \sqrt{\frac{v}{v^2 - a^2}}\sqrt{\frac{k^2 v}{4(v^2 - a^2)} - g + \frac{j}{J}\left[v(w_r - v) - a^2\right]}\right]^2 \quad . \quad (5.45)$$

5.4.2 Stagnation Point Analysis

At the stagnation point, $v = 0$, several terms in the equation of motion grow without bound. The equation here becomes dominated by the two sound-speed terms in this limit:

$$F_1 \approx -\frac{a^2}{v}\left(\frac{dv}{dr}\right)_o + \frac{ja^2}{J} = 0 \quad , \quad (5.46)$$

but this is just an expression of L'Hôpital's rule, because, as $v \to 0$, $J \to 0$, and

$$\frac{j(r)v(r)}{J(r)} \to \frac{j(r)(dv/dr) + v(r)(dj/dr)}{dJ/dr} \to \frac{dv}{dr} \quad . \quad (5.47)$$

Although this implies that solutions passing through the stagnation point may be non-unique, this *exact* cancellation of the sound-speed terms is fortuitous because it allows us to ignore these terms in the analysis of the overall disk dynamics. This is analogous to the zero-sound-speed approximation in the standard CAK analysis (Section 2.3.2), which is valid in most of the wind.

To better obtain a physical understanding of the "mass loading" source term in the radial momentum equation, let us also momentarily ignore the *radiative forces* and the effects of rotation. Although the use of this assumption would not reproduce full numerical models of wind compressed disks (i.e., OCB), we find that the solution topology of these one-dimensional disk winds is quite complex even without radiation forces and rotation. It is important to first understand the effects of the source terms in isolation before considering the full problem. The equation of motion, then, is approximated by

$$v\frac{dv}{dr} + g - \frac{jv(w_r - v)}{J} = 0 \quad , \quad (5.48)$$

where here $g = GM_*/r^2$. If we demand a finite acceleration through the stagnation point r_o, L'Hôpital's rule provides the value of the velocity gradient and surface density there:

$$\left(\frac{dv}{dr}\right)_o = \frac{g(r_o)}{w_r(r_o)} \quad , \qquad \sigma_o = \frac{j_o(r_o)\, w_r(r_o)}{g(r_o)} \quad . \tag{5.49}$$

The only unknown quantity here is the value of r_o itself, but a reasonably good approximate value is given by the peak of $j(r)$ in, e.g., Figure 5.9.

Let us examine the solution topology of the above differential equation by writing it in dimensionless form; i.e., by defining the variables

$$x \equiv 1 - \frac{r_o}{r} \quad , \qquad y \equiv \frac{v}{\sqrt{GM_*/r_o}} \quad , \qquad \tilde{w} \equiv \frac{w_r}{\sqrt{GM_*/r_o}} \tag{5.50}$$

where x ranges from a negative constant $(1 - r_o/R_*)$ at the stellar surface, through zero at the stagnation point, to unity as $r \to \infty$. The variables y and $\tilde{w}$ are scaled to an escape-speed-like quantity at the stagnation point. For simplicity let us also assume that j and $\tilde{w}$ are *constants* in the wind, implying that $J \approx j(r_o)(r - r_o)$ in the vicinity of the stagnation point. The equation of motion is then given by

$$y\frac{dy}{dx} = -1 + \frac{y(\tilde{w} - y)}{x(1-x)} \quad , \tag{5.51}$$

or in a more standard form for nonlinear differential equations,

$$\frac{dy}{dx} = \frac{x(x-1) + y(\tilde{w} - y)}{xy(1-x)} \quad . \tag{5.52}$$

There are four *singular points* of this equation, where both the numerator and denominator approach zero:

1. $(x = 0, y = 0)$: This is the stagnation point, where L'Hôpital's rule gives the finite velocity gradient

$$\frac{dy}{dx} = \frac{1}{\tilde{w}} \quad , \tag{5.53}$$

which agrees with eq. (5.49) above. However, solutions of infinite slope are also formally possible at this point, implying that the stagnation point is a "nodal" type singular point with a very pathological nature (see, e.g., Holzer 1977).

2. $(x = 1, y = 0)$: This is a threshold point at which the wind *decelerates* to zero velocity at $r \to \infty$, and the finite velocity gradient is a mirror image of the above:

$$\frac{dy}{dx} = -\frac{1}{\tilde{w}} \quad . \tag{5.54}$$

This nodal point also admits infinite-slope solutions.

3. $(x = 0, y = \tilde{w})$: This solution is uninteresting in the present analysis because it implies full "entrainment" of the disk velocity at the *external* wind velocity at the stagnation radius, and this is not expected to occur.

4. $(x = 1, y = \tilde{w})$: This "attractor"-like point represents full entrainment as $r \rightarrow \infty$, which is a realistic assumption for winds that actually are propelled to infinity by the external wind source terms.

Figure 5.10 shows the solution topology for this simplified form of the equation of motion for two values of $\tilde{w}$ on opposite sides of unity. The dotted lines are loci of *zero slope* solutions (i.e., when the numerator of eq. [5.52] vanishes), and the four singular points are also intercepted by these loci. Solutions which pass through the stagnation point ($x = 0$, $y = 0$) attempt to stay on the finite-slope solution $dy/dx = 1/\tilde{w}$, but any infinitesimal perturbation makes them switch to near-infinite slope solutions, branching off in an unstable way. Solutions which *decelerate* from the finite-slope line receive a slight enhancement in the surface density σ, and this eventually amplifies into an over-dense solution that must decelerate to zero velocity (and possibly "crash" back down in a time-dependent manner). Solutions which *accelerate* from the finite-slope line grow less dense, and thus may be able to accelerate out to infinity if there is sufficient added momentum from the source term. This multiplicity of possible solutions is a direct result of the nonlinearities in the governing ODE, and when more realistic physics is incorporated, this degeneracy may be lifted.

Note that for the $\tilde{w} = 0.8$ topology there is insufficient momentum being added to the wind to accelerate any solutions to infinity, and all velocity laws $y(x)$ which pass through the stagnation point eventually decelerate to zero velocity. For the $\tilde{w} = 1.2$ topology, however, some solutions have enough momentum to counteract gravity and accelerate to the "entrainment" velocity $y = \tilde{w}$ at $x = 1$. The fact that $\tilde{w}$ is scaled to the *escape speed* at r_o provides the physical justification of only $\tilde{w} \gtrsim 1$ solutions being able to entrain disk solutions to infinity.

Radii beneath the stagnation point, for which we assume the velocity is directed inwards toward the star (i.e., $x < 0$, $y < 0$) exhibit different types of solutions from the above. Despite the existence of infinite-slope solutions immediately below the stagnation radius, a stable and convergent decelerating solution appears to exist when integrating *downward* from $x = 0$. Because the majority of the mass-loading occurs around the stagnation point, the solutions at lower x values are causally determined from higher radii, and the stability of this part of the velocity law seems assured.

The obvious next step in this analysis would be to consider the radiative driving and centrifugal terms in the equation of motion, but at this preliminary stage

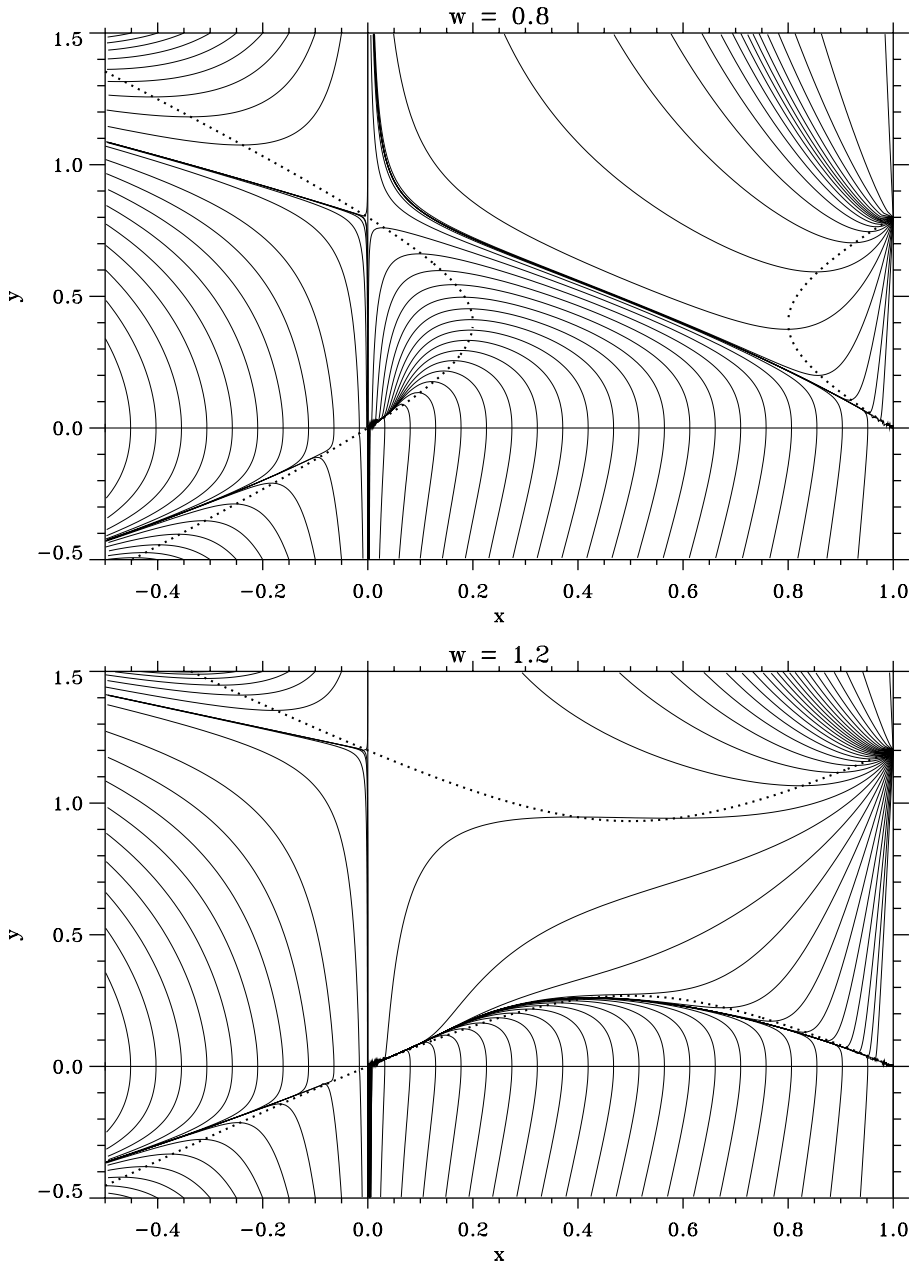

Figure 5.10: Solution topology to the dimensionless 1D wind compressed disk equation of motion, without radiation or centrifugal forces. The upper curve shows a *small* value of the external wind velocity (0.8); a situation where not enough momentum is provided to propel the wind to infinity. The lower curve shows a *large* value of the external wind velocity (1.2); a situation where the wind can be propelled to infinity, but some decelerating solutions are still possible.

we have not yet explored these effects. To zero order, we expect that radiative forces should not be extremely important in very *dense* wind compressed disks (because of the $\rho^{-\alpha}$ dependence in the Sobolev line force). However, for observed B-star rotation rates, OCB found that actual WCDs are only enhanced in density by factors of 10–100 over the polar wind, and radiative forces in the disk may be significant. Certainly the presence of another outward force would help the radial velocity in WCDs to accelerate out to infinity, and possibly may lift the solution degeneracy around the stagnation point.

Finally, then, the utility of this one-dimensional model of a disk must be critically examined. The two-dimensional numerical hydrodynamics solutions show the disk velocity laws to be quite stable and well-behaved. Thus, if the extreme instability and degeneracy of the 1D solutions persists when all relevant physics has been included, then the only remaining difference between the methods is the treatment of the *latitudinal* direction. It may be the case that the only accurate way to study the phenomenon of WCD formation is in two dimensions, with the "source terms" modeled self-consistently, together with the disk. This would represent the failure of the present 1D formalism, but no matter the outcome, we will have learned a great deal about the physics of wind-fed disks around rotating stars from this attempt.